

1 Automatic discrimination of underwater acoustic
2 signals generated by teleseismic P-waves: A
3 probabilistic approach

Alexey Sukhovich,¹ Jean-Olivier Irisson,^{2,3} Frederik J. Simons,⁴ Anthony
Ogé,¹ Yann Hello,¹ Anne Deschamps,¹ and Guust Nolet¹

A. Sukhovich, Géoazur, Observatoire Océanologique de Villefranche-sur-Mer, 2 quai de la Darse, BP 48-06235 Villefranche-sur-Mer, France. (alexey.sukhovich@geoazur.obs-vlfr.fr)

J.-O. Irisson, Observatoire Océanologique, Station Zoologique, B.P. 28, Chemin du Lazaret 06230 Villefranche-sur-Mer, France.

F. J. Simons, Department of Geosciences, Princeton University, Princeton NJ, USA.

A. Ogé, Géoazur, Observatoire Océanologique de Villefranche-sur-Mer, 2 quai de la Darse, BP 48-06235 Villefranche-sur-Mer, France.

Y. Hello, Géoazur, Observatoire Océanologique de Villefranche-sur-Mer, 2 quai de la Darse, BP 48-06235 Villefranche-sur-Mer, France.

A. Deschamps, Géoazur, 250, Rue Albert Einstein, 06560 Sophia Antipolis, France.

G. Nolet, Géoazur, 250, Rue Albert Einstein, 06560 Sophia Antipolis, France.

¹Géoazur, Sophia Antipolis, France.

4 We propose a new probabilistic scheme for the automatic recognition of
5 underwater acoustic signals generated by teleseismic P-waves recorded by
6 hydrophones in the ocean. The recognition of a given signal is based on the
7 relative distribution of its power among different frequency bands. The sig-
8 nal's power distribution is compared with a statistical model developed by
9 analyzing relative power distributions of many signals of the same origin and
10 a numerical criterion is calculated, which can serve as a measure of the prob-
11 ability for the signal to belong to the statistical model. Our recognition scheme
12 was applied to 6-month-long continuous records of seven ocean bottom hy-
13 drophones (OBH) deployed in the Ligurian Sea. A maximum of 94% of all
14 detectable teleseismic P-waves recorded during the deployment of the OBHs
15 were recognized correctly with no false recognitions. The proposed recogni-

²UPMC Univ Paris 06, UMR 7093, LOV,
Observatoire océanologique, F-06234,
Villefranche-sur-Mer, France

³CNRS, UMR 7093, LOV, Observatoire
océanologique, F-06234,
Villefranche-sur-Mer, France

⁴Department of Geosciences, Princeton
University, Princeton NJ, USA.

16 tion method will be implemented in autonomous underwater robots dedi-
17 cated to detect and transmit acoustic signals generated by teleseismic P-waves.

1. Introduction

18 Currently, there is a lack of seismic data collected over oceanic regions. The scarcity
19 of seismic records from the oceans hampers the progress of global seismic tomography,
20 especially when one attempts imaging of the Southern hemisphere, which contains most
21 of the known hotspots. The present approach to seismic data collection in the oceans
22 includes the use of ocean bottom seismometers [*Webb, 1998; Stephen et al., 2003*] and
23 moored hydrophones [*Fox et al., 2001; Dziak et al., 2004*]. However, high installation
24 and data recovery costs render these instruments too expensive to allow for a coverage
25 that is sufficiently dense for the purposes of global seismic tomography. Teleseismic P-
26 waves arriving at the ocean bottom are refracted into the water column and generate
27 acoustic signals, which are of particular interest as their arrival times can be used in
28 seismic tomography. *Simons et al. [2009]* have proposed to use autonomous freely-drifting
29 underwater robots (called MERMAID, short for Mobile Earthquake Recording in Marine
30 Areas by Independent Divers) equipped with hydrophones. By changing its buoyancy,
31 the robot is able to dive to and remain at a certain depth. While at depth, the robot
32 continuously monitors the pressure variation by calculating the ratio of short-term to long-
33 term moving averages (STA/LTA algorithm) [*Allen, 1978*]. We wish that, once a strong
34 teleseismic P-wave is detected, the robot immediately begins an ascent to establish satellite
35 connection for the transmission of the recorded waveform. However, in oceanic domains
36 there are many detectable acoustic signals generated by sources other than teleseismic
37 earthquakes (e.g. ships, air gun campaigns, T-waves, marine animals). As each diving/re-
38 surfacing cycle depletes the MERMAID's battery, it is of utmost importance to ensure

39 that the robot surfaces only in case of a strong teleseismic P-wave detection. In this paper,
40 we report on the development of a new probabilistic scheme that allows the automatic
41 discrimination of teleseismic P-waves while missing very few of them and at the same time
42 maintaining the probability of false recognitions at a minimum.

2. Method

43 Our method begins with the analysis of a detected signal to obtain the distribution
44 of its power among different frequency bands. This distribution is then compared to a
45 statistical model for signals of a given type to calculate a numerical criterion, which can
46 be regarded as a probability for the signal to be of this type. Based on the value of the
47 criterion, the decision is taken on whether the MERMAID will or will not ascend.

48 To obtain information on how the power of the signal is split among frequency bands, we
49 use the discrete wavelet transform (DWT). Wavelet analysis has several advantages over
50 conventional Fourier transforming of overlapping time windows. Just as the spectrogram,
51 wavelet analysis provides information on both time behavior and frequency content of
52 a signal. However, the DWT is non-redundant; it generates exactly as many wavelet
53 coefficients as there are samples in the signal and thus requires fewer calculations. At
54 the same time, simple and easy-to-program algorithms exist for calculating the DWT.
55 In particular, we are using the “lifting” algorithm [*Sweldens*, 1996]. By removing small-
56 magnitude, statistically unimportant wavelet coefficients, it is also possible to compress
57 the signal and thus significantly reduce the amount of the data transmitted via satellite,
58 as shown in the analysis by *Simons et al.* [2009]. Finally, the DWT can be performed
59 in integer arithmetic with little or no loss of accuracy, which helps to reduce the power

60 consumption by the central processing unit (CPU). To improve accuracy of the integer
61 DWT, we have modified the normalization part of the lifting algorithm, which originally
62 involved division and multiplication by an irrational number. The details can be found in
63 the supplementary material.

64 In the wavelet transform analysis, the notion of frequency is replaced by the notion of a
65 “scale”. In a sense, the wavelet transformation is analogous to a filter-bank analysis, with
66 overlapping filters covering different frequency bands [*Jensen and la Cour-Harbo*, 2001].
67 During wavelet transformation, every iteration produces a set of wavelet coefficients for
68 each scale, which in its turn corresponds to a particular frequency band. As a rule of
69 thumb, each subsequent scale has a passband centered around a frequency that is half of
70 the center frequency of the previous scale. There exist many wavelet bases, among which
71 the most suitable one can be chosen for the problem at hand. We use a biorthogonal
72 wavelet basis with two and four vanishing moments for the primal and dual wavelets re-
73 spectively, which is commonly abbreviated as CDF(2,4) [*Cohen et al.*, 1992]. As *McGuire*
74 *et al.* [2008] found, this wavelet construction provides a very good compromise between
75 computational effort and the filtering performance of the wavelets.

76 The result of the wavelet analysis is most conveniently visualized by means of a scalo-
77 gram, which presents the absolute values of the wavelet coefficients in the time-scale
78 plane. The scalograms of representative signals of four different types analyzed in this
79 paper are shown in Figure 1. We estimate the power of the detected signal at any scale
80 by calculating the average of absolute values of its wavelet coefficients:

$$s_k = \frac{1}{N_k} \sum_{i=1}^{N_k} |w_i^k| , \quad (1)$$

81 where w_i^k is a wavelet coefficient, N_k is the number of the wavelet coefficients and indexes
 82 i and k number time and scale, respectively. Strictly speaking, the estimate of the signal
 83 power should be done by calculating the average of the squares of wavelet coefficients;
 84 however, our definition is better suited for the calculations when the minimization of
 85 energy consumption is required. Equation (1) is evaluated for wavelet coefficients within
 86 a time window, whose limits are defined by the instances at which the STA/LTA ratio
 87 rises over 2 (trigger threshold) and then drops below 1 (de-trigger threshold). Note that
 88 after a trigger occurs, the LTA is still updated and thus affected by the triggering signal.
 89 By applying Equation (1) to each scale, we obtain a set of scale averages s_k . To find the
 90 *relative* power distribution among the scales, the scale averages are normalized by their
 91 L_1 norm:

$$\tilde{s}_k = \frac{s_k}{L_1} , \text{ where } L_1 = \sum_{k=1}^K s_k . \quad (2)$$

92 In our case the number of scales K equals 6. We subsequently divide each element \tilde{s}_k
 93 by the corresponding element \tilde{n}_k of the similar scale average calculated for the ambient
 94 noise record preceding the time of the STA/LTA trigger:

$$S_k = \frac{\tilde{s}_k}{\tilde{n}_k} . \quad (3)$$

95 To better estimate the values of \tilde{n}_k , the scale averages are calculated for several over-
96 lapping noise records (512-samples-long taken with 10% overlap) and averaged to give
97 a single element \tilde{n}_k used in Equation (3). This second normalization by ambient noise
98 means that a pure noise record with no signal should give elements S_k with values close to
99 1 for all scales. For brevity, in the rest of the paper we will refer to the normalized scale
100 averages S_k as simply “scale averages”, while the term “normalized” should be implied.

101 In order to derive statistical properties of signals of a certain origin, the scale averages
102 S_k are calculated for as many pre-identified signals as possible and their distributions are
103 obtained for each scale. We call this set of distributions the “statistical model” for the
104 signals of this type (Figure 2). The recognition is performed by comparing the values
105 of scale averages S_k^0 calculated for a detected signal with the statistical model for the
106 signals generated by teleseismic P-waves. For each scale k , we compute the proportion
107 p_k of the model scale averages S_k more extreme than S_k^0 (i.e. $S_k > S_k^0$ when S_k^0 lies to
108 the right of the median and $S_k < S_k^0$ when S_k^0 lies to the left of the median); in other
109 words, we estimate the area of the tail of the distribution beyond S_k^0 . This is similar to
110 quantifying the probability of committing an error known in statistics as a Type I error,
111 which here means rejecting the signal as not belonging to the category of interest while it
112 does. When S_k^0 is close to the median of the distribution, the probability of committing
113 the Type I error is high since many S_k values are more extreme than S_k^0 and thus the
114 computed proportion is high. We take the high probability of the Type I error as an
115 indication that the detected signal is likely to be of the same origin as that of the signals
116 used to create the statistical model. Conversely, when S_k^0 is located near one of the tails

117 of the distribution, the probability of wrongly rejecting the signal is low. This serves as
 118 an indication that the signal is likely to be of a different origin.

119 To combine the information from the various scales, multiplying the proportions would
 120 compute the probability to obtain a signal more extreme at *all* scales, which is too restric-
 121 tive. Instead, we have found it to be much more effective to calculate a weighted average
 122 of p_k to obtain a single criterion C , ranging between 0 and 1 and quantifying the overall
 123 agreement between the detected signal and the statistical model:

$$C = \frac{\sum_k p_k D_k}{\sum_k D_k} \quad . \quad (4)$$

124 where weights D_k are quantified by the Kolmogorov-Smirnov statistic [*Press et al.*, 1992];
 125 more details on their calculation are given in the supplementary material. When C is
 126 higher than a given threshold, we accept the signal as being a P-wave.

127 The complement to the Type I error is the Type II error, i.e. the error of accepting
 128 the detected signal as belonging to the model while it does not. This error would cause
 129 the MERMAID to surface and transmit a signal generated by a source other than a
 130 teleseismic P-wave. We refer to such recognition as a “false positive”. Minimizing or
 131 eliminating false positives is critically important for reducing the power consumption and
 132 thus for the overall success of the MERMAID’s mission. We discuss our approach to
 133 ensure the absence of Type II errors after the presentation of our data analysis.

3. Data

134 To determine the optimum threshold for C and to test the method, we have used
 135 continuous records of seven High Tech HTI-01-PCA hydrophones deployed at the bottom

136 of the Ligurian Sea during the Grosmarin experiment, which was conducted between the
137 end of April and the beginning of October 2008 [Dessa *et al.*, 2011]. The hydrophones
138 were installed at distances ranging between 18 and 52 km from the coast and at depths
139 ranging between 1300 and 2400 m within a square area of approximately $37.5 \text{ km} \times 50 \text{ km}$
140 near (8.00E, 43.5N). The sampling rate was 100 Hz.

141 To keep our analysis as close as possible to an actual mission of the MERMAID, the
142 Grosmarin data were downsampled to 40 Hz after low-pass filtering with a numerical filter
143 whose transfer function closely approximated the analogue 10 Hz low-pass filter installed
144 on the MERMAID. Because of this low-pass filter, we did not consider the first scale of
145 the wavelet transforms.

146 The Grosmarin data set was very useful for the development of the method since it
147 contains a large variety of noise signals detectable by the STA/LTA algorithm. First, cruise
148 ships and ferries passed several times a day over the area of instruments' deployment. Also,
149 the installation of the OBHs was followed by a continuous 3-day-long campaign of seismic
150 shots using Bolt air guns which generated a large number of acoustic signals arriving at
151 hydrophones from many angles and distances.

4. Results

152 During the Grosmarin experiment, a total of 131 acoustic signals unambiguously gen-
153 erated by teleseismic P-waves were recorded and then used to produce a statistical model
154 for teleseismic P-waves. These signals were identified by predicting the arrival times of
155 the P-waves for known earthquakes. In addition, we have also created statistical models
156 for three other types of signals which are most likely to be encountered by the MERMAID

157 during an actual long-time mission: signals produced by air guns, passing ships and T-
158 waves. The ship and T-wave signals were identified by eye. As explained in Section 2,
159 the scale averages for each signal were normalized by the scale averages of the preceding
160 noise record. Therefore, the statistical model for the ambient noise was created as a ref-
161 erence model allowing us to validate the normalization by the ambient noise. This model
162 was obtained by randomly choosing a large number of ambient noise record pairs (512-
163 samples-long) from the full Grosmarin database and calculating normalized scale averages
164 for each pair. All statistical models are shown in Figure 2.

165 The statistical model describes how *on average* the power of the signals of a given
166 origin is split among different scales (or equivalently, frequency bands). From Figure 2
167 it is already clear by eye that the power of the two types of geophysical interest (P-
168 and T-waves) is distributed significantly differently from each other and from signals of
169 other origins. The fact that ship signals are statistically close to the ambient noise may
170 indicate a relatively high contribution of ships to the ambient noise. The inspection of
171 the statistical model for teleseismic P-waves shows that most of the power is concentrated
172 in scales 5 and 6, as expected for teleseismic events of large magnitude [Aki, 1967]. Also,
173 all median values of the ambient noise model are very close to unity, as expected.

174 After the recognition criterion C for a given signal is obtained, we must decide which
175 numerical value should be taken as an indicator of a teleseismic P-wave detection with
176 high probability. To this end, we simulated the MERMAID's mission by running the
177 STA/LTA algorithm on the full Grosmarin database and calculated C for each detected

178 signal using the P-wave statistical model. In addition to C , we calculated signal-to-noise
 179 ratio (SNR) values defined as:

$$SNR = \frac{\sum_{k=2}^K s_k}{\sum_{k=2}^K n_k} \quad . \quad (5)$$

180 where s_k and n_k are given by Equation (1). A total of 176 signals were detected by the
 181 STA/LTA algorithm. Figure 3 shows the detected signals according to their C and SNR
 182 values. It is evident that most of the signals of non-P-wave origin (lower panel of Figure 3)
 183 with high value of C have low values of SNR . At the same time, the non-P-wave signals
 184 with high SNR have very low values of C . Therefore, by choosing thresholds for both C
 185 and SNR , we can eliminate false positive recognitions. With thresholds $C_0 = 0.15$ and
 186 $SNR_0 = 2.25$, 94% (61 out of 65) of detected P-wave signals are recognized correctly with
 187 no false positives. Even with more conservative thresholds $C_0 = 0.2$ and $SNR_0 = 3.1$,
 188 which would further limit the possibility of false positive recognitions, the recognition rate
 189 of P-wave signals was still 69%. Although there is no guarantee that false positives will
 190 be completely eliminated in a future independent data set, the choice of C_0 and SNR_0 is
 191 obviously a good one. In MERMAID deployments we plan to use the most conservative
 192 thresholds to decide if the robot should surface immediately upon a teleseismic P-wave
 193 detection, while using C to rank less certain detections by their priority in a (finite)
 194 buffer for transmission at the next surfacing. The exact values of the thresholds are
 195 yet to be determined; in fact, we are still in the process of collecting noise data before
 196 committing ourselves to a fixed strategy. The lateral drift during an ascent of about 2.5
 197 hours depends on the local oceanic currents and is at most a few hundred meters so that

198 the GPS location upon surfacing should be accurate enough for the seismic tomography.
199 The geolocation of the stored events will require interpolation (e.g. *Taillandier et al.*,
200 2006). To keep interpolation errors acceptable, the robot will surface at least every 10–15
201 days, depending on location.

202 All detected signals with high SNR (> 5) but not originating from teleseismic P-waves
203 (lower panel in Figure 3), are ruled out even with a very moderate threshold $C_0 = 0.1$.
204 We found that most of these strong signals were T-waves. The T-waves are expected to
205 be frequently detected by the MERMAIDs whose programmed parking depth (around
206 1500 m) at low- and mid-latitudes will be within the depth range of the axis of the Sound
207 Fixing And Ranging channel, where T-waves propagate over long distances with very little
208 attenuation [*Dziak et al.*, 2004]. Since T-waves are unsuitable for seismic tomography, it
209 is very important that our method is able to eliminate them with high efficiency.

210 As a final test, we have applied the recognition method to an independent data set
211 obtained with the same instrument as in the Grosmarin experiment, but deployed near
212 coast of Haiti (72.97W, 18.62N) at the depth of 1508 m during a 4-month-long period
213 after the devastating earthquake in January 2010. By using the statistical model for P-
214 waves obtained from the Grosmarin data and the thresholds $C_0 = 0.15$ and $SNR_0 =$
215 2.25 we recognized 75% (21 out of 28) of teleseismic P-wave signals with only two false
216 positives. One of these false positives was produced by a high-amplitude spike signal due
217 to electronic noise. The other much weaker signal, although closely resembling a P-wave,
218 was tentatively classified as a false positive since we were not able to identify its source

219 earthquake. The application of more conservative thresholds $C_0 = 0.2$ and $SNR_0 = 3.1$
220 resulted in 46% of correct recognitions while ruling out the tentative false positive.

221 The statistical models presented in this paper were developed from the data recorded
222 by instruments used during the Grosmarin experiment. One would expect that the nor-
223 malization by a preceding ambient noise record will render the method insensitive to
224 instrument response. However, a wavelet decomposition is not equivalent to a Fourier
225 transform, and one can show that the instrument response does not divide out perfectly
226 during the normalization. In addition, care should be taken not to include scales that
227 are mostly outside the passband of the instrument. Finally, the noise characteristics may
228 be different depending on geographical location. We therefore recommend not to blindly
229 adopt the criteria developed in this paper (although they may provide a good starting
230 point in most cases), but to perform an analysis separately for each pool of equivalent
231 instruments and for each geographical location, if possible.

232 It seems worthwhile comparing our recognition scheme with other existing methods
233 applicable to an automatic recognition of teleseismic events. Similar to our method, all
234 of them analyze both time and frequency properties of seismograms. *Evans and Allen*
235 [1983] use two STA/LTA ratios calculated simultaneously for high-passed and low-passed
236 versions of a seismogram, and call an event detected when triggering for the low-passed
237 version but not for the high-passed one. *Goforth and Herrin* [1981] compute coefficients
238 of the Walsh transform (which in a broad sense is analogous to Fourier transform) of
239 overlapping time windows. The distribution of the absolute values of the coefficients cor-
240 responding to the frequency band of interest is obtained and detection is declared when

241 the similar sum for subsequent time windows falls out of a pre-set confidence interval.
242 *Gledhill* [1985] uses Discrete Fourier Transform on a 10-s-long time window to estimate
243 spectral power within five equal frequency bands and compares band levels with average
244 band levels obtained from similar analysis on preceding 512 time windows. The above
245 methods are similar in that they all use negative decision logic, i.e. the detection is de-
246 clared based on the detected deviations from the ambient noise. Our approach is different
247 as we test for positive correlation between a signal and a given statistical model. In this
248 sense, our method is similar to the one by *Joswig* [1990], whose recognition algorithm
249 tests the degree of correlation between a continuously updated pattern of a seismogram
250 and patterns corresponding to the signals of known origins. However, his patterns (two-
251 dimensional gray scale pictures) are calculated from scaled spectrograms whose calculation
252 involves significantly larger amount of computations as compared to the DWT [*Simons*
253 *et al.*, 2009]. Our method thus seems to be better suited for platforms with limited power
254 supply such as MERMAIDs. Finally, to the best of our knowledge, our method is the
255 first one which utilizes the probabilistic approach and allows to estimate the probability
256 of false positive recognitions.

257 Note that our method is not limited to the recognition of teleseismic P-waves. Provided
258 the statistical model of the signals whose automatic recognition is sought is sufficiently
259 different from those of the signals of other types (most likely to be encountered by a
260 detecting instrument) the proposed recognition method should work. In particular, the
261 method seems to be readily applicable to the automatic recognition of T-waves (Figure 2).

5. Conclusions

262 We have presented a new method for the automatic recognition of underwater acoustic
263 signals generated by teleseismic P-waves. The method is based on the analysis of the
264 relative power distribution among different frequency bands and utilizes the DWT as a
265 signal processing tool. By analyzing the relative power distributions of a large number of
266 P-wave signals, we derived a statistical model for P-waves. The resemblance between a
267 detected signal and the statistical model is quantified by the criterion C , which is akin to
268 a probability of committing the Type I error during recognition (i.e. rejecting a P-wave
269 signal while it should be accepted). It was also shown that the SNR of the analyzed signal
270 can be used as an additional recognition criterion and can help eliminate false positive
271 recognitions. Our method is not limited to the recognition of teleseismic P-waves and
272 can be applied to the recognition of any signals whose statistical models differ sufficiently
273 from those of other intervening signals.

274 **Acknowledgments.** We wish to thank J. Perrot for helpful discussions on T-waves.
275 This work is was supported by European Research Council (Advanced grant 226837) and
276 by Marie Curie Re-integration grant (project 223799).

References

- 277 Aki, K. (1967), Scaling law of seismic spectrum, *J. Geophys. Res.*, *72*(4), 1217–1231.
278 Allen, R. V. (1978), Automatic earthquake recognition and timing from single traces,
279 *Bull. Seismol. Soc. Am.*, *68*(5), 1521–1532.

- 280 Cohen, A., I. Daubechies, and J. Feauveau (1992), Biorthogonal bases of compactly sup-
281 ported wavelets, *Comm. Pure Appl. Math.*, *45*, 485–560.
- 282 Dessa, J.-X., S. Simon, M. Lelièvre, M.-O. Beslier, A. Deschamps, N. Béthoux, S. So-
283 larino, F. Sage, E. Eva, G. Ferretti, O. Bellier, and C. Eva (2011), The Grosmarin
284 Experiment: Three dimensional crustal structure of the North Ligurian margin from
285 refraction tomography and preliminary analysis of microseismic measurements, *Bull.*
286 *Soc. Géol. France*, in press.
- 287 Dziak, R. P., D. R. Bohnenstiehl, H. Matsumoto, C. G. Fox, D. K. Smith, M. Tolstoy,
288 T.-K. Lau, J. H. Haxel, and M. J. Fowler (2004), *P*- and *T*-wave detection thresholds,
289 *Pn* velocity estimate, and detection of lower mantle and core *P*-waves on ocean sound-
290 channel hydrophones at the Mid-Atlantic Ridge, *Bull. Seismol. Soc. Am.*, *94*(2), 665–
291 677.
- 292 Evans, J., and S. S. Allen (1983), A teleseism-specific detection algorithm for single short
293 period traces, *Bull. Seismol. Soc. Am.*, *73*(4), 1173–1186.
- 294 Fox, C. G., H. Matsumoto, and T.-K. A. Lau (2001), Monitoring pacific ocean seismicity
295 from an autonomous hydrophone array, *J. Geophys. Res.*, *106*(B3), 1347–1352.
- 296 Gledhill, K. R. (1985), An earthquake detector employing frequency domain techniques,
297 *Bull. Seismol. Soc. Am.*, *75*(6), 1827–1835.
- 298 Goforth, T., and E. Herrin (1981), An automatic seismic signal detection algorithm based
299 on the walsh transform, *Bull. Seismol. Soc. Am.*, *71*(4), 1351–1360.
- 300 Jensen, A., and A. la Cour-Harbo (2001), *Ripples in Mathematics*, Springer, Berlin.

- 301 Joswig, M. (1990), Pattern recognition for earthquake detection, *Bull. Seismol. Soc. Am.*,
302 *80*(1), 170–186.
- 303 McGuire, J. J., F. J. Simons, and J. A. Collins (2008), Analysis of seafloor seismograms
304 of the 2003 Tokachi-Oki earthquake sequence for earthquake early warning, *Geophys.*
305 *Res. Lett.*, *35*, L14310, doi:10.1029/2008GL033986.
- 306 Press, W., S. Teukolsky, W. Vetterling, and B. Flannery (1992), *Numerical Recipes*, second
307 ed., Cambridge University Press, Cambridge, UK.
- 308 Simons, F. J., G. Nolet, P. Georgief, J. M. Babcock, L. A. Regier, and R. E. Davis
309 (2009), On the potential of recording earthquakes for global seismic tomography by
310 low-cost autonomous instruments in the oceans, *J. Geophys. Res.*, *114*, B05307, doi:
311 10.1029/2008JB006088.
- 312 Stephen, R. A., F. N. Spiess, J. A. Collins, J. A. Hildebrand, J. A. Orcutt, K. R. Peal, F. L.
313 Vernon, and F. B. Wooding (2003), Ocean seismic network pilot experiment, *Geochem.*
314 *Geophys. Geosyst.*, *4*, 1092.
- 315 Sweldens, W. (1996), The lifting scheme: A custom-design construction of biorthogonal
316 wavelets, *Appl. Comput. Harmon. Anal.*, *3*(2), 186–200.
- 317 Taillandier, V., A. Griffa, P.-M. Poulain, and K. Béranger (2006), Assimilation of Argo
318 float positions in the north western Mediterranean Sea and impact on ocean circulation
319 simulations, *Geophys. Res. Lett.*, *33*, L11604, doi:10.1029/2005GL025552.
- 320 Webb, S. C. (1998), Broadband seismology and noise under the ocean, *Reviews of Geo-*
321 *physics*, *36*(1), 105–142.

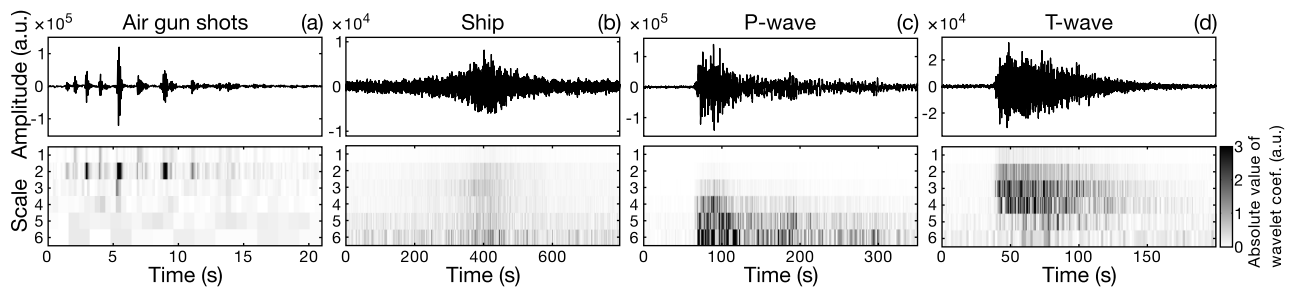


Figure 1. Representative acoustic signals generated by (a) an air gun, (b) a passing ship, (c) a teleseismic P-wave and (d) a T-wave with their scalograms. Each pixel in a scalogram represents the absolute value of a wavelet coefficient (arbitrary scale). The sampling rate of the signals is 40 Hz. The effective frequency range is thus between 0 and 20 Hz. The first scale of the DWT corresponds approximately to a passband covering the upper half of the original frequency range, i.e. to 10–20 Hz; the second scale corresponds to 5–10 Hz, and so on. Note that most of the power of the teleseismic P-wave signal is at scales 5 and 6, which jointly cover the low frequency range between approximately 0.30 and 1.25 Hz, as expected.

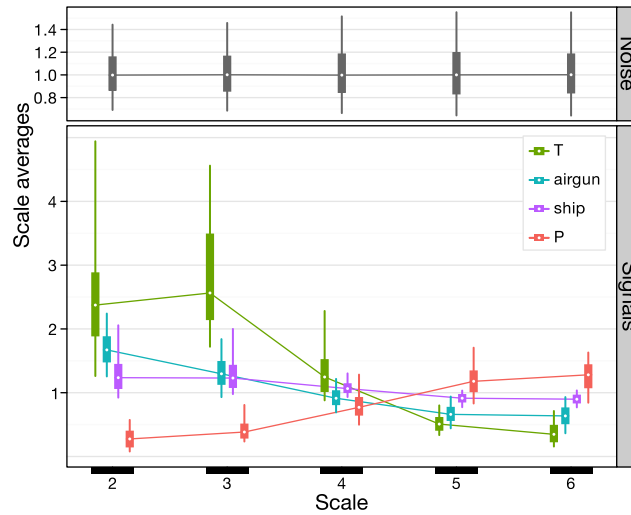


Figure 2. Description of the statistical models (top) for the ambient noise and (bottom) for the four types of signals recorded during the Grosmarin experiment. For each distribution of scale averages, the center point denotes the median, the box is delimited by the 25% and 75% quantiles and the vertical line ranges from the 5% to the 95% quantiles. The lines joining the medians of the distributions serve only as a guide for the eye.

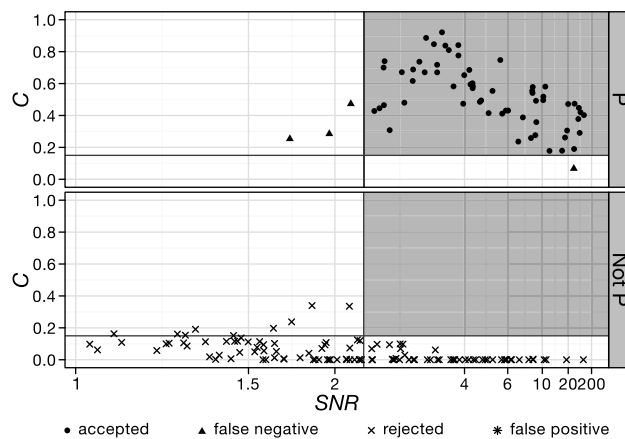


Figure 3. Positions of the signals, recorded during the Grosmarin experiment, in (C, SNR) space. Note that the SNR scale is not linear to better spread the points. Top panel shows teleseismic P-wave signals while the bottom panel shows all other signals. The figures allow visualization of the choice of thresholds for C and SNR in order to simultaneously maximize the number of correct recognitions and to minimize (or eliminate completely) the number of false positives. The shaded region on top and bottom figures is defined by the values of $C_0 = 0.15$ and $SNR_0 = 2.25$.